# INVERSE MEDIUM SCATTERING PROBLEMS IN NEAR-FIELD OPTICS[*1)]

Gang Bao

(*Department of Mathematics, Michigan State University, East Lansing, MI 48824, USA*
*Email: bao@math.msu.edu*)

Peijun Li

(*Department of Mathematics, University of Michigan, Ann Arbor, MI 48109, USA*
*Email: lipeijun@umich.edu*)

**Abstract**

A regularized recursive linearization method is developed for a two-dimensional inverse medium scattering problem that arises in near-field optics, which reconstructs the scatterer of an inhomogeneous medium deposited on a homogeneous substrate from data accessible through photon scanning tunneling microscopy experiments. In addition to the ill-posedness of the inverse scattering problems, two difficulties arise from the layered background medium and limited aperture data. Based on multiple frequency scattering data, the method starts from the Born approximation corresponding to the weak scattering at a low frequency, each update is obtained via recursive linearization with respect to the wavenumber by solving one forward problem and one adjoint problem of the Helmholtz equation. Numerical experiments are included to illustrate the feasibility of the proposed method.

*Mathematics subject classification:* 78A46, 65N21.
*Key words:* Inverse medium scattering, Helmholtz equation, Near-field optics, Recursive linearization.

## 1. Introduction

Scattering problems are basic in many scientific research areas such as radar, sonar, geophysical exploration, medical imaging, and nondestructive testing [1–3]. In near-field optics, the scattering problems further involve wave fields containing evanescent components to improve resolution [4,5], which arise naturally in diverse applications such as the imaging of biological samples, the inspection and manipulation of nano-electronic components in semiconductor technology, and the inspection and activation of nano-optical devices [6]. Near-field optics has attracted considerable attention as an effective approach to obtain images with subwavelength resolution [7].

Three important modalities that fall in the scenario of near-field optics are near-field scanning optical microscopy (NSOM) [8], total internal reflection microscopy (TIRM) [9,10], and photon scanning tunneling microscopy (PSTM) [11,12]. In NSOM, the light source is transmitted through both the fiber and the small aperture at the tip of a probe. The probe is scanned over the sample in the near-field zone. The field scattered by the sample is then collected and measured in the far-field zone as a function of the probe position. In TIRM, the sample is

---

illuminated by high spatial frequency evanescent plane waves, which may be generated by total internal reflection from a prism [13]. The scattered field is measured in the far zone of the sample as the direction of the incident wave is varied. In PSTM, the sample is illuminated by an evanescent field generated at the face of a prism (similar to TIRM), but the scattered field is detected via a tapered fiber probe in the near zone of the sample (as in NSOM). See [6] for an account of other modalities as basic experiments of near-field optics and associated scattering theories.

In all of the above mentioned modalities, it is desirable to solve the inverse scattering problem in order to reconstruct the sample from the measured data. Initial results in this direction have been reported in the cases of three-dimensional inhomogeneous media for all of the three modalities: NSOM [8] , TIRM [9], and more recently PSTM [11]. The basic idea is to develop an analytical solution technique for solving the linearized inverse scattering problem for each modality within the framework of the weak scattering approximation. Numerical solution of the nonlinear inverse problem is at present completely open. The main purpose of the present work is to explore the possibility of developing a regularized recursive linearization approach for solving the nonlinear inverse scattering problem in the modality of PSTM. It should be pointed out that we currently adopt the non-global approach, *i.e.*, the scattered field resulting from the interaction of the incident field with the sample is analyzed in the absence of the tip. This procedure overlooks the possible influence of the tip on the detected field. The global approach which takes into account the entire system is the subject of future work.

The remainder of this paper is organized as follows. The mathematical model of the scattering problems is introduced in Section 2. Based on the Lippmann–Schwinger integral equation in a two-layered background medium, an initial guess of the reconstruction is derived from the Born approximation corresponding to the weak scattering at a low frequency in Section 3. In Section 4, a regularized recursive linearization algorithm is proposed. Numerical examples are presented in Section 5. The paper is concluded with some general remarks and directions for future research in Section 6.

## 2. Model Problem

Consider an inhomogeneous sample deposited on a homogeneous substrate, usually a prism. The substrate is assumed to be relatively thick so that only one face needs to be considered, thus defining an interface between two half-spaces. The index of refraction in the lower half-space (substrate) has a constant value $n_0$. However, the index of refraction in the upper half-space varies within the domain of the sample but otherwise has a value of unity. The sample is illuminated from below (transmission geometry) by a time-harmonic plane wave, as shown in Fig. 2.1. Throughout, by assuming nonmagnetic materials and transverse electric polarization, the model PDE reduces to the two-dimensional Helmholtz equation.

More specifically, let an incoming plane wave $u^{\mathrm{i}} = \exp(i\alpha x_1 + i\beta x_2)$ be incident on the straight line $\{x_2 = 0\}$ from $\mathbb{R}^2_- = \{\mathbf{x} : x_2 < 0\}$, where

$$\alpha = n_0 k \sin\theta, \quad \beta = n_0 k \cos\theta, \quad \theta \in (-\pi/2, \pi/2),$$

and $k$ is the free space wavenumber. The total field $u$ satisfies the Helmholtz equation:

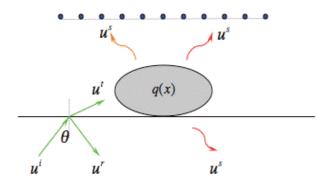$$\Delta u + n^2 k^2 (1 + q) u = 0, \tag{2.1}$$

Fig. 2.1. The geometry of the problem. A plane wave is incident on the prism from the bottom. The scatterer is illuminated by the transmitted waves and the scattered waves are measured in the constant height configuration by an idealized point detector in the near zone.

where the scatterer $q(\mathbf{x})$ has a compact support contained in $D \subseteq \mathbb{R}^2_+ = \{\mathbf{x} : x_2 > 0\}$ and

$$
n(\mathbf{x}) = \begin{cases} 1 & \text{for } x_2 > 0, \\ n_0 & \text{for } x_2 < 0. \end{cases}
$$

Denote the reference field $u^{\text{ref}}$ as the solution of the homogeneous equation:

$$
\Delta u^{\text{ref}} + n^2 k^2 u^{\text{ref}} = 0. \tag{2.2}
$$

It can be analytically obtained from Eq. (2.2) together with continuity conditions that

$$
u^{\text{ref}} = \begin{cases} u^{\text{t}} & \text{for } x_2 > 0, \\ u^{\text{i}} + u^{\text{r}} & \text{for } x_2 < 0, \end{cases}
$$

where $u^{\text{t}}$ and $u^{\text{r}}$ are the transmitted and reflected waves, respectively [14, 15]. More precisely, we have

$$
u^{\text{t}} = T \exp(i\alpha x_1 + i\gamma x_2) \quad \text{and} \quad u^{\text{r}} = R \exp(i\alpha x_1 - i\beta x_2), \tag{2.3}
$$

where $T = 2\beta/(\beta + \gamma), R = (\beta - \gamma)/(\beta + \gamma)$, and

$$
\gamma(\alpha) = \begin{cases} \sqrt{k^2 - \alpha^2} & \text{for } k > |\alpha|, \\ i\sqrt{\alpha^2 - k^2} & \text{for } k < |\alpha|. \end{cases}
$$

The total field consists of the reference field $u^{\text{ref}}$ and the scattered field $u^{\text{s}}$:

$$
u = u^{\text{ref}} + u^{\text{s}}. \tag{2.4}
$$

It follows from (2.1), (2.2), and (2.4) that the scattered field satisfies

$$
\Delta u^{\text{s}} + n^2 k^2 (1 + q) u^{\text{s}} = -k^2 q u^{\text{t}}. \tag{2.5}
$$

In addition, the scattered field is required to satisfy the following radiation condition [16]

$$
\lim_{R \to \infty} \int_{\Sigma_R} \left| \frac{\partial u^{\text{s}}}{\partial \nu} - i n k u^{\text{s}} \right|^2 dS = 0,
$$

where $\Sigma_R$ is the sphere of radius $R$ and $\nu$ is the unit outward normal to $\Sigma_R$.

Given the reference field $u^{\text{ref}}$, the forward problem is to determine the scattered field $u^{\text{s}}$ for the known scatterer $q$, which has been well studied [16–20]. The inverse problem is to determine the scatterer $q$ from the measurements of the scattered field $u^{\text{s}}$, for the given reference field $u^{\text{ref}}$. The scattered field is measured by an idealized point detector at $\{\mathbf{x}_j : x_{2j} = b\}, j = 1, \cdots, m$, where $b$ is a constant. In addition to the ill-posedness of the inverse scattering problem, two difficulties arise from the layered background medium and limited aperture data. In particular, the open domain with a two-layered background medium needs to be truncated into a bounded computational domain. For the forward solver, we apply the finite element method with a perfectly matched layer technique to truncate the unbounded domain [21–24]. The inverse scattering problem with limited aperture data is challenging, since without full aperture measurements, the ill-posedness and nonlinearity of the inverse problem become more severe. In the full aperture case, stable and efficient recursive linearization methods were proposed for solving the two-dimensional Helmholtz equation [25] and the three-dimensional Maxwell equations [26], respectively. A homotopy continuation method with limited aperture data but in a homogeneous background medium may be found in [27].

In this work, we develop a regularized recursive linearization to solve the inverse scattering problem of the two-dimensional Helmholtz equation in a two-layered background medium with limited aperture data. The algorithm requires multiple frequency scattering data, and the recursive linearization is obtained by a continuation method on the wavenumber. It first solves a linear equation (Born approximation) at the lowest wavenumber. Updates are subsequently obtained by using a sequence of increasing wavenumbers. Following the idea of the Kaczmarz method [3, 28–30], we use partial data to perform the Landweber iteration at each wavenumber. At each iteration, one forward problem and one adjoint problem of the Helmholtz equation are solved.

## 3. Born Approximation

In this section, a starting point is derived for the iteratively recursive linearization algorithm based on the linearized Lippmann–Schwinger integral equation. The Lippman–Schwinger integral equation and the fundamental solution, $G(\mathbf{x}, \mathbf{y})$, for the Helmholtz equation in a two-layered background medium are given in the appendix.

When the wavenumber $k$ is small, the scattered field is weak [31]. By dropping the scattered field at the right hand side of (A8) under the weak scattering, we obtain the linearized integral equation

$$u^{\text{s}}(\mathbf{x}) = k^2 \int_D G(\mathbf{x}, \mathbf{y}) q(\mathbf{y}) u^{\text{t}}(\mathbf{y}) d\mathbf{y}, \tag{3.1}$$

which is the well known Born approximation.

It follows from the scattered field measured at $x_2 = b$ that

$$u^{\text{s}}(x_1, b) = k^2 \int_{-\infty}^{\infty} dy_1 \int_0^b dy_2 \, G(x_1, b; y_1, y_2) u^{\text{t}}(y_1, y_2) q(y_1, y_2). \tag{3.2}$$

Substituting the explicit form of the transmitted field (2.3) and the fundamental solution (A6),

and realizing the dependence of the scattered field $u^{\mathrm{s}}$ on $\alpha$, we may rewrite (3.2) as

$$
\begin{aligned}
u^{\mathrm{s}}(x_1; \alpha) =& \frac{ik^2 T}{4\pi} \int_{-\infty}^{\infty} dy_1 \int_0^b dy_2 \, \exp(i\alpha y_1 + i\gamma y_2) q(y_1, y_2) \\
& \times \int_{-\infty}^{\infty} d\xi \, \frac{\exp(i\beta_1 b)}{\beta_1} \left[ \frac{\beta_1 - \beta_2}{\beta_1 + \beta_2} \exp(i\beta_1 y_2) + \exp(-i\beta_1 y_2) \right] \exp(i\xi(x_1 - y_1)), \quad (3.3)
\end{aligned}
$$

where $\beta_1$ and $\beta_2$ are defined in the appendix. Rearranging the integral order, we obtain

$$
\begin{aligned}
u^{\mathrm{s}}(x_1; \alpha) =& \frac{ik^2 T}{4\pi} \int_0^b dy_2 \, \exp(i\gamma y_2) \int_{-\infty}^{\infty} d\xi \, \frac{\exp(i\beta_1 b)}{\beta_1} \left[ \frac{\beta_1 - \beta_2}{\beta_1 + \beta_2} \exp(i\beta_1 y_2) + \exp(-i\beta_1 y_2) \right] \\
& \times \exp(i\xi x_1) \int_{-\infty}^{\infty} dy_1 \, \exp(-i(\xi - \alpha)y_1) q(y_1, y_2). \quad (3.4)
\end{aligned}
$$

Noting the last integral is the Fourier transform of the scatterer with respect to $y_1$,

$$
\begin{aligned}
u^{\mathrm{s}}(x_1; \alpha) =& \frac{ik^2 T}{4\pi} \int_0^b dy_2 \, \exp(i\gamma y_2) \int_{-\infty}^{\infty} d\xi \, \frac{\exp(i\beta_1 b)}{\beta_1} \left[ \frac{\beta_1 - \beta_2}{\beta_1 + \beta_2} \exp(i\beta_1 y_2) + \exp(-i\beta_1 y_2) \right] \\
& \times \exp(i\xi x_1) \hat{q}(\xi - \alpha, y_2). \quad (3.5)
\end{aligned}
$$

Multiplying both sides of (3.5) by $\exp(-i\omega x_1)$, integrating with respect to $x_1$, and observing that

$$
\frac{1}{2\pi} \int_{-\infty}^{\infty} \exp(i\omega x_1) dx_1 = \delta(\omega),
$$

we obtain the Fourier transform of scattered field with respect to $x_1$

$$
\begin{aligned}
\hat{u}^{\mathrm{s}}(\omega; \alpha) =& \frac{ik^2 T}{2} \int_0^b dy_2 \, \exp(i\gamma y_2) \int_{-\infty}^{\infty} d\xi \, \frac{\exp(i\beta_1 b)}{\beta_1} \left[ \frac{\beta_1 - \beta_2}{\beta_1 + \beta_2} \exp(i\beta_1 y_2) + \exp(-i\beta_1 y_2) \right] \\
& \times \delta(\xi - \omega) \hat{q}(\xi - \alpha, y_2), \quad (3.6)
\end{aligned}
$$

which gives rise to

$$
\begin{aligned}
\hat{u}^{\mathrm{s}}(\omega; \alpha) =& \frac{ik^2 T}{2} \int_0^b dy_2 \, \frac{\exp(i\beta_1(\omega)b)}{\beta_1(\omega)} \left[ \frac{\beta_1(\omega) - \beta_2(\omega)}{\beta_1(\omega) + \beta_2(\omega)} \exp(i\beta_1(\omega)y_2) + \exp(-i\beta_1(\omega)y_2) \right] \\
& \times \exp(i\gamma y_2) \hat{q}(\omega - \alpha, y_2). \quad (3.7)
\end{aligned}
$$

When $|\omega| < k$ and $|\alpha| < k$, both $\beta_1$ and $\gamma$ are real numbers. The Fourier transform may be used for Eq. (3.7) to produce an approximation of the scatterer $q$. In this case, the inversion involves data related to the scatterer through the Fourier transform in the case of weak scattering. The reconstructed Fourier modes of $q$ at most fill the disk of radius $2k$. See [32] for an detailed resolution analysis of the Born approximation in the homogeneous background medium. However, for $k < |\alpha| < n_0 k$, $\gamma$ is a pure imaginary number. From (3.7), it is easily seen that the inversion involves data related to the scatterer through a Fourier–Laplace transform in the case of weak scattering, due to the presence of the evanescent waves. For each $|\omega| < k$ and $|\alpha| < n_0 k$, it follows from $|\omega - \alpha| < (n_0 + 1)k$ that the Fourier modes of the reconstructed scatterer may be beyond the $2k$ along the transverse part of $y_1$.

Introduce the integral kernel

$$
\begin{aligned}
K(\omega, \alpha; y_2) =& \frac{ik^2 T \exp(i\beta_1(\omega)b)}{2\beta_1(\omega)} \left[ \frac{\beta_1(\omega) - \beta_2(\omega)}{\beta_1(\omega) + \beta_2(\omega)} \exp(i\beta_1(\omega)y_2) + \exp(-i\beta_1(\omega)y_2) \right] \\
& \times \exp(i\gamma(\alpha)y_2).
\end{aligned}
$$

The integral equation (3.7) can be written as

$$\hat{u}^{\mathrm{s}}(\omega; \alpha) = \int_0^b K(\omega, \alpha; y_2) \hat{q}(\omega - \alpha; y_2) dy_2. \tag{3.8}$$

By denoting $\xi = \omega - \alpha$, we can formally rewrite (3.8) as

$$K(\xi)\hat{q}(\xi) = \hat{u}^{\mathrm{s}}(\xi). \tag{3.9}$$

In practice, Eq. (3.9) is implemented by using the method of least squares with Tikhonov regularization [33]

$$\hat{q}(\xi) = (\lambda I + K^* K)^{-1} K^* \hat{u}^{\mathrm{s}}(\xi), \tag{3.10}$$

where $\lambda$ is a small positive number, $I$ is the identity operator, and $K^*$ is the adjoint operator of $K$. Once $\hat{q}(\xi, y_2)$ is available, an approximation of $q$ may be obtained from the inverse Fourier transform.

## 4. Recursive Linearization

As discussed in the previous section, when the wavenumber $k$ is small, the Born approximation allows a reconstruction of those low Fourier modes for the function $q$. We now describe a procedure that recursively determines better approximations $q_k$ at $k = k_l$ for $l = 1, 2, \cdots$ with the increasing wavenumbers. Suppose now that an approximation of the scatterer, $q_{\tilde{k}}$, has been recovered at some wavenumber $\tilde{k}$, and that the wavenumber $k$ is slightly larger that $\tilde{k}$. We wish to determine $q_k$, or equivalently, to determine the perturbation

$$\delta q = q_k - q_{\tilde{k}}.$$

For the reconstructed scatterer $q_{\tilde{k}}$, we solve at the wavenumber $k$ the forward scattering problem

$$\Delta \tilde{u}_i^{\mathrm{s}} + n^2 k^2 (1 + q_{\tilde{k}}) \tilde{u}_i^{\mathrm{s}} = -k^2 q_{\tilde{k}} u_i^{\mathrm{t}}, \tag{4.1}$$

where $u_i^{\mathrm{t}}$ is the transmitted wave corresponding to the incident wave $u_i^{\mathrm{i}}$ with incident angle $\theta_i, i = 1, \cdots, p$.

For the scatterer $q_k$, we have

$$\Delta u_i^{\mathrm{s}} + n^2 k^2 (1 + q_k) u_i^{\mathrm{s}} = -k^2 q_k u_i^{\mathrm{t}}. \tag{4.2}$$

Subtracting (4.1) from (4.2) and omitting the second order smallness in $\delta q$ and in $\delta u_i^{\mathrm{s}} = u_i^{\mathrm{s}} - \tilde{u}_i^{\mathrm{s}}$, we obtain

$$\Delta \delta u_i^{\mathrm{s}} + n^2 k^2 (1 + q_{\tilde{k}}) \delta u_i^{\mathrm{s}} = -k^2 \delta q (u_i^{\mathrm{t}} + \tilde{u}_i^{\mathrm{s}}). \tag{4.3}$$

Given a solution $u_i^{\mathrm{s}}$ of (4.2), we define the measurements

$$M u_i^{\mathrm{s}}(\mathbf{x}) = [u_i^{\mathrm{s}}(\mathbf{x}_1), \cdots, u_i^{\mathrm{s}}(\mathbf{x}_m)]^T. \tag{4.4}$$

The measurement operator $M$ is well defined and maps the scattered field to a vector of complex numbers in $\mathbb{C}^m$, which consists of point measurements of the scattered field at $\mathbf{x}_j, j = 1, \cdots, m$.

For the scatterer $q_k$ and the transmitted field $u_i^{\mathrm{t}}$, we define the forward scattering operator

$$S(q_k, u_i^{\mathrm{t}}) = M u_i^{\mathrm{s}}. \tag{4.5}$$

It is easily seen that the forward scattering operator $S(q_k, u_i^{\mathrm{t}})$ is linear with respect to $u_i^{\mathrm{t}}$ but nonlinear with respect to $q_k$. For simplicity, we denote $S(q_k, u_i^{\mathrm{t}})$ by $S_i(q_k)$. Let $S_i^{'}(q_{\tilde{k}})$ be the Fréchet derivative of $S_i(q_k)$ and denote the residual operator

$$R_i(q_{\tilde{k}}) = M(\delta u_i^{\mathrm{s}}). \tag{4.6}$$

It follows from the linearization of the nonlinear equation (4.5) that

$$S_i^{'}(q_{\tilde{k}})\delta q = R_i(q_{\tilde{k}}). \tag{4.7}$$

Applying the Landweber iteration [33] to the linearized equation (4.7) yields

$$\delta q = \tau S_i^{'}(q_{\tilde{k}})^* R_i(q_{\tilde{k}}), \tag{4.8}$$

where $\tau$ is a positive relaxation parameter and $S_i^{'}(q_{\tilde{k}})^*$ is the adjoint operator of $S_i^{'}(q_{\tilde{k}})$.

In order to compute the correction $\delta q$, we need some efficient way to compute $S_i^{'}(q_{\tilde{k}})^* R_i(q_{\tilde{k}})$. Let $R_i(q_{\tilde{k}}) = [\zeta_{i1}, \cdots, \zeta_{im}]^T \in \mathbb{C}^m$. Consider the adjoint problem

$$\Delta \psi_i + n^2 k^2 (1 + q_{\tilde{k}})\psi_i = -k^2 \sum_{j=1}^{m} \zeta_{ij} \delta(\mathbf{x} - \mathbf{x}_j). \tag{4.9}$$

Multiplying (4.3) with the complex conjugate of $\psi_i$ and integrating over $\mathbb{R}^2$ on both sides, we obtain

$$\int_{\mathbb{R}^2} \Delta \delta u_i^{\mathrm{s}} \overline{\psi}_i d\mathbf{x} + \int_{\mathbb{R}^2} n^2 k^2 (1 + q_{\tilde{k}})\delta u_i^{\mathrm{s}} \overline{\psi}_i d\mathbf{x} = -k^2 \int_{\mathbb{R}^2} \delta q(u_i^{\mathrm{t}} + \tilde{u}_i^{\mathrm{s}}) \overline{\psi}_i d\mathbf{x}.$$

Using Green's formula for an infinite space, we have

$$\int_{\mathbb{R}^2} \left(\Delta \overline{\psi}_i + n^2 k^2 (1 + q_{\tilde{k}})\overline{\psi}_i\right) \delta u_i^{\mathrm{s}} d\mathbf{x} = -k^2 \int_{\mathbb{R}^2} \delta q(u_i^{\mathrm{t}} + \tilde{u}_i^{\mathrm{s}}) \overline{\psi}_i d\mathbf{x}.$$

It follows from the adjoint equation (4.9) that

$$\sum_{j=1}^{m} \delta u_i^{\mathrm{s}}(\mathbf{x}_j)\overline{\zeta}_{ij} = \int_{\mathbb{R}^2} \delta q(u_i^{\mathrm{t}} + \tilde{u}_i^{\mathrm{s}}) \overline{\psi}_i d\mathbf{x}. \tag{4.10}$$

Noting (4.6), (4.7), and the adjoint operator $S_i^{'}(q_{\tilde{k}})^*$, the left-hand side of (4.10) may be deduced

$$\sum_{j=1}^{m} \delta u_i^{\mathrm{s}}(\mathbf{x}_j)\overline{\zeta}_{ij} = \langle M(\delta u_i^{\mathrm{s}}), R_i(q_{\tilde{k}})\rangle_{\mathbb{C}^m} = \langle S_i^{'}(q_{\tilde{k}})\delta q, R_i(q_{\tilde{k}})\rangle_{\mathbb{C}^m}$$

$$= \langle \delta q, S_i^{'}(q_{\tilde{k}})^* R_i(q_{\tilde{k}})\rangle_{L^2(\mathbb{R}^2)} = \int_{\mathbb{R}^2} \delta q \, \overline{S^{'}(q_{\tilde{k}})^* R_i(q_{\tilde{k}})} d\mathbf{x}. \tag{4.11}$$

where $\langle \cdot, \cdot \rangle_{\mathbb{C}^m}$ and $\langle \cdot, \cdot \rangle_{L^2(\mathbb{R}^2)}$ are the standard inner-products defined in the complex vector space $\mathbb{C}^m$ and the square integrable functional space $L^2(\mathbb{R}^2)$ .

Combining (4.10) and (4.11) yields

$$\int_{\mathbb{R}^2} \delta q \, \overline{S^{'}(q_{\tilde{k}})^* R_i(q_{\tilde{k}})} d\mathbf{x} = \int_{\mathbb{R}^2} \delta q \, (u_i^{\mathrm{t}} + \tilde{u}_i^{\mathrm{s}}) \overline{\psi}_i d\mathbf{x},$$

which holds for any $\delta q$. It follows that

$$S^{'}(q_{\tilde{k}})^* R_i(q_{\tilde{k}}) = (\overline{u_i^{\mathrm{t}}} + \overline{\tilde{u}^{\mathrm{s}}}) \psi_i. \tag{4.12}$$
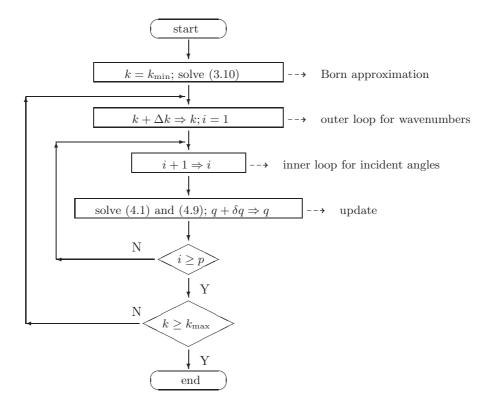
Fig. 4.1. The flow chart of the recursive linearization algorithm.

Using the above result, Eq. (4.8) can be written as

$$\delta q = \tau(\overline{u_i^{\mathrm{t}}} + \overline{\tilde{u}_i^{\mathrm{s}}})\,\psi_i. \tag{4.13}$$

Thus, for each incident wave, we solve one forward problem (4.1) and one adjoint problem (4.9). Once $\delta q$ is determined, $q_k$ is updated by $q_{\tilde{k}} + \delta q$. After completing the $p$th sweep, we get the reconstructed scatterer $q_k$ at the wavenumber $k$.

Given the data of the scattered field $u_i^{\mathrm{s}}(\mathbf{x}_j), j = 1, \cdots, m, i = 1, \cdots, p$ at different wavenumbers from the smallest $k_{\min}$ to the largest $k_{\max}$, a flow chart of the recursive linearization algorithm is given in Fig. 4.1.

## 5. Numerical Experiments

In the following, to illustrate the performance of our algorithm, we present two numerical examples. The scattering data are obtained by numerical solution of the forward scattering problem, which is implemented by using the finite element method with a perfectly matched layer technique.

The index of refraction $n_0 = 2$ in the lower half-space prism and the relaxation parameter $\tau$ is taken to be $0.1/k^2$. The scattered field are measured on $\mathbf{x}_j = (x_{1j}, 1.0), x_{1j} = -0.5 + j/40, j = 0, \cdots, 40$, and the incident angle $\theta_i = -2\pi/5 + i4\pi/50, i = 0, \cdots, 10$. Evidently, the incident waves consist of the evanescent plane waves and the propagating plane waves. For stability analysis, some relative random noise is added to the data, *i.e.,* the scattered field takes the
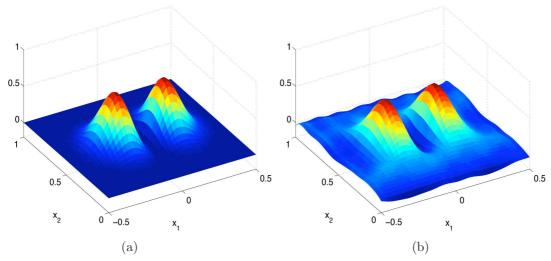
Fig. 5.1. Example 5.1: (a) the true scatterer; (b) the reconstructed scatterer.

form
$$u_i^s(\mathbf{x}_j) := (1 + \sigma \, \mathrm{rand}) u_i^s(\mathbf{x}_j), \quad j = 0, \cdots, 40, \quad i = 0, \cdots, 10.$$

Here, rand gives uniformly distributed random numbers in $[-1, 1]$ and $\sigma$ is a noise level parameter taken to be 0.02 in our numerical experiments. Define the relative error by

$$e_2 = \frac{(\sum_{i,j} |q_{ij} - \tilde{q}_{ij}|^2)^{1/2}}{(\sum_{i,j} |q_{ij}|^2)^{1/2}},$$

where $\tilde{q}$ is the reconstructed scatterer and $q$ is the true scatterer.

**Example 5.1.** Let $q(x_1, x_2) = 2x_1^2 \exp(-x_1^2 - x_2^2)$, and reconstruct a scatterer defined by

$$q_1(x_1, x_2) = q(6x_1, 6(x_2 - 0.5)) \tag{5.1}$$

inside the domain $D = [-0.5, 0.5] \times [0.0, 1.0]$. See Figs. 5.1(a) and 5.2(a) for the surface plot and the image of the function. Figs. 5.1(b) and 5.2(b) show the surface plot and the image of the final reconstruction at the wavenumber $k = 12$. Fig. 5.3 presents the relative error of reconstructions at different wavenumbers with step size of the wavenumber $\Delta k = 1$ and $\Delta k = 2$.

**Example 5.2.** Let $q(x_1, x_2) = 2x_2^2 \exp(-x_1^2 - x_2^2)$, and reconstruct a scatterer defined by

$$q_2(x_1, x_2) = q(6x_1, 6(x_2 - 0.5)) \tag{5.2}$$

inside the domain $D = [-0.5, 0.5] \times [0.0, 1.0]$. See Figs. 5.4(a) and 5.5(a) for the surface plot and the image of the function. It is important to note that the two isolated peaks in this example lie along the direction of the $x_2$-axis instead of the $x_1$-axis as shown in Example 5.1. Figs. 5.4(b) and 5.5(b) show the surface plot and the image of the final reconstruction at the wavenumber $k = 12$. Fig. 5.6 presents the relative error of reconstructions at different wavenumbers with step size of the wavenumber $\Delta k = 1$ and $\Delta k = 2$. The two peaks reconstructed in Example 5.2 are not as well separated as that of Example 5.1, as seen in Figs. 5.2(b) and 5.5(b). Comparing the reconstructions of Examples 5.1 and 5.2, it is clear that better resolution is achieved along

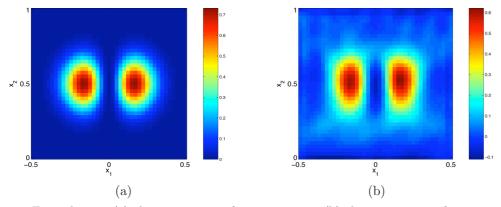(a)                                                    (b)

Fig. 5.2. Example 5.1: (a) the image view of true scatterer; (b) the image view of reconstructed scatterer.



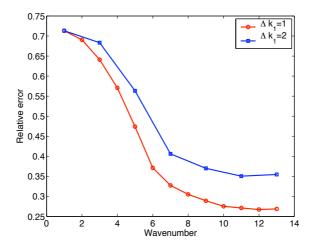Fig. 5.3. Example 5.1: the relative error of reconstruction at different wavenumbers.



(a)                                                    (b)
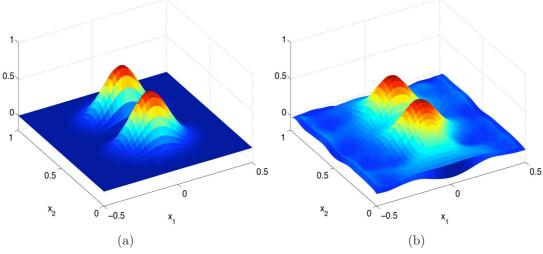
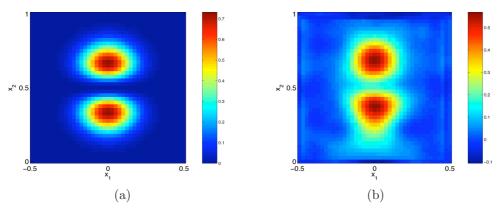Fig. 5.4. Example 5.2: (a) the true scatterer; (b) the reconstructed scatterer.

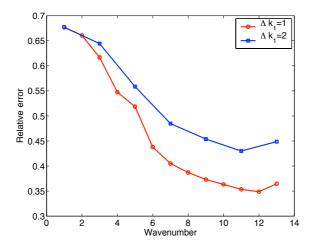Fig. 5.5. Example 5.2: (a) the image view of true scatterer; (b) the image view of reconstructed scatterer.



Fig. 5.6. Example 5.2: the relative error of reconstruction at different wavenumbers.

the $x_1$-axis than that along the $x_2$-axis since the evanescent waves propagate along the $x_1$-axis but exponentially decay along the $x_2$-axis. Due to the noise added to the scattering data, the semiconvergence of the iterative algorithm can be clearly observed in Fig. 5.6, *i.e.*, the algorithm firstly converges to certain level and then starts to diverge. This phenomenon further illustrates the ill-posedness of the inverse scattering problem. In practice, if the noise level is known, the discrepancy principle may be used as a stopping rule for detecting the transient from convergence to divergence [33].

# 6. Conclusion

We have presented a regularized recursive linearization method for reconstructing the scatterer of inhomogeneities in the modality of PSTM. The proposed method is stable and efficient for solving the inverse medium scattering in the layered background medium with limited aperture measurements. There are two important future directions of the present study. The first concerns the convergence analysis of the recursive linearization algorithm, which is in progress and will be reported elsewhere. Another research direction is concerned with a detailed study

of the resolution of the proposed method and extend the approach in this paper further to the more complicated 3D model problems.

# Appendix

## A. Lippmann–Schwinger Integral Equation

For the observation point $\mathbf{x} = (x_1, x_2)$ and the source point $\mathbf{y} = (y_1, y_2)$, the fundamental solution of the Helmholtz equation, $G(\mathbf{x}, \mathbf{y})$, in a two-layered background medium in $\mathbb{R}^2$ satisfies

$$\Delta G(\mathbf{x}, \mathbf{y}) + n^2(\mathbf{x})k^2 G(\mathbf{x}, \mathbf{y}) = -\delta(\mathbf{x} - \mathbf{y}) \tag{A.1}$$

with continuity conditions

$$G(\mathbf{x}, \mathbf{y})|_{x_2=0^+} = G(\mathbf{x}, \mathbf{y})|_{x_2=0^-}, \tag{A.2}$$

$$\left.\frac{\partial G(\mathbf{x}, \mathbf{y})}{\partial x_2}\right|_{x_2=0^+} = \left.\frac{\partial G(\mathbf{x}, \mathbf{y})}{\partial x_2}\right|_{x_2=0^-}, \tag{A.3}$$

where $\delta$ is the Dirac delta function.

Define

$$\beta_1(\xi) = \begin{cases} \sqrt{k^2 - \xi^2} & \text{for } |k| > |\xi|, \\ i\sqrt{\xi^2 - k^2} & \text{for } |k| < |\xi|, \end{cases}$$

and

$$\beta_2(\xi) = \begin{cases} \sqrt{(n_0 k)^2 - \xi^2} & \text{for } |n_0 k| > |\xi|, \\ i\sqrt{\xi^2 - (n_0 k)^2} & \text{for } |n_0 k| < |\xi|. \end{cases}$$

It follows from the Fourier transform of (A1) as suggested in [14, 34] and the integral representation of the Hankel function [35, 36] that

- $x_2 > 0$, $y_2 < 0$

$$G(\mathbf{x}, \mathbf{y}) = \frac{i}{2\pi} \int_{-\infty}^{\infty} \frac{e^{i(\beta_1 x_2 - \beta_2 y_2)}}{\beta_1 + \beta_2} e^{i\xi(x_1 - y_1)} d\xi, \tag{A.4}$$

- $x_2 < 0$, $y_2 > 0$

$$G(\mathbf{x}, \mathbf{y}) = \frac{i}{2\pi} \int_{-\infty}^{\infty} \frac{e^{i(\beta_1 y_2 - \beta_2 x_2)}}{\beta_1 + \beta_2} e^{i\xi(x_1 - y_1)} d\xi, \tag{A.5}$$

- $x_2 > 0$, $y_2 > 0$

$$G(\mathbf{x}, \mathbf{y}) = \frac{i}{4\pi} \int_{-\infty}^{\infty} \frac{1}{\beta_1} \left[ \frac{\beta_1 - \beta_2}{\beta_1 + \beta_2} e^{i\beta_1(x_2 + y_2)} + e^{i\beta_1 |x_2 - y_2|} \right] e^{i\xi(x_1 - y_1)} d\xi, \tag{A.6}$$

- $x_2 < 0$, $y_2 < 0$

$$G(\mathbf{x}, \mathbf{y}) = \frac{i}{4\pi} \int_{-\infty}^{\infty} \frac{1}{\beta_2} \left[ \frac{\beta_2 - \beta_1}{\beta_1 + \beta_2} e^{-i\beta_2(x_2 + y_2)} + e^{i\beta_2 |x_2 - y_2|} \right] e^{i\xi(x_1 - y_1)} d\xi. \tag{A.7}$$

Using the fundamental solution (A4)-(A7), we obtain from (2.5) that the scattered field $u^{\mathrm{s}}$ satisfies

$$u^{\mathrm{s}}(\mathbf{x}) = k^2 \int_D G(\mathbf{x}, \mathbf{y}) q(\mathbf{y})(u^{\mathrm{t}}(\mathbf{y}) + u^{\mathrm{s}}(\mathbf{y})) d\mathbf{y}. \tag{A.8}$$

Adding the transmitted field $u^{\mathrm{t}}$ on both sides of (A8) yields the total field in $\mathbb{R}^2_+$

$$u(\mathbf{x}) = u^{\mathrm{t}}(\mathbf{x}) + k^2 \int_D G(\mathbf{x}, \mathbf{y}) q(\mathbf{y}) u(\mathbf{y}) d\mathbf{y}, \tag{A.9}$$

which gives the Fredholm integral equation of the second kind for the total field in $D$

$$u(\mathbf{x}) - k^2 \int_D G(\mathbf{x}, \mathbf{y}) q(\mathbf{y}) u(\mathbf{y}) d\mathbf{y} = u^{\mathrm{t}}(\mathbf{x}). \tag{A.10}$$

Once the total field in $D$ is computed, the total field can be directly obtained from

$$u(\mathbf{x}) = u^{\mathrm{t}}(\mathbf{x}) + k^2 \int_D G(\mathbf{x}, \mathbf{y}) q(\mathbf{y}) u(\mathbf{y}) d\mathbf{y} \quad \text{for } \mathbb{R}^2_+ \setminus D, \tag{A.11}$$

and

$$u(\mathbf{x}) = u^{\mathrm{i}}(\mathbf{x}) + u^{\mathrm{r}}(\mathbf{x}) + k^2 \int_D G(\mathbf{x}, \mathbf{y}) q(\mathbf{y}) u(\mathbf{y}) d\mathbf{y} \quad \text{for } \mathbf{x} \in \mathbb{R}^2_-. \tag{A.12}$$

# References

[1] D. Colton and R. Kress, Integral Equation Methods in Scattering Theory, Wiley, New York, 1983.

[2] D. Colton and R. Kress, Inverse Acoustic and Electromagnetic Scattering Theory, Springer-Verlag, Berlin, 1998.

[3] F. Natterer, The Mathematics of Computerized Tomography, Teubner, Stuttgart, 1986.

[4] D. Courjon and C. Bainier, Near field microscopy and near field optics, *Rep. Prog. Phys.*, **57** (1994), 989-1028.

[5] C. Giard and A. Dereux, Near-field optics theories, *Rep. Prog. Phys.*, **59** (1996), 657-699.

[6] P. Carney and J. Schotland, Near-field tomography, in Inside Out: Inverse Problems and Applications, G. Uhlmann (Ed.), Cambridge University Press, 2003, 133-168.

[7] D. Courjon, Near-field Microscopy and Near-field Optics, Imperial College Press, London, 2003.

[8] P. Carney and J. Schotland, Inverse scattering for near-field microscopy, *Appl. Phys. Lett.*, **77** (2000), 2798-2800.

[9] P. Carney and J. Schotland, Three-dimensional total internal reflection microscopy, *Opt. Lett.*, **26** (2001), 1072-1074.

[10] P. Carney and J. Schotland, Theory of total-internal-reflection tomography, *J. Opt. Soc. Am. A*, **20** (2003), 542-547.

[11] P. Carney and J. Schotland, Determination of three-dimensional structure in photon scanning tunneling microscopy, *J. Opt. A: Pure Appl. Opt.*, **4** (2002), s140-s144.

[12] D. Courjon, K. Sarayeddine and M. Spajer, Scanning tunneling optical microscopy, *Opt. Commun.*, **71** (1989), 23-28.

[13] P.A. Temple, Total internal reflection microscopy: a surface inspection technique, *Appl. Opt.*, **20** (1981), 2656-2664.

[14] I. Akduman and A. Alkumru, A generalized ART algorithm for inverse scattering problems related to buried cylindrical bodies, *Inverse Probl.*, **11** (1995), 1125-1136.

[15] M. Idemen and I. Akduman, Two-dimensional inverse scattering problems connected with bodies buried in a slab, *Inverse Probl.*, **6** (1990), 749-766.

[16] P.-M. Cutzach and C. Hazard, Existence, uniqueness and analyticity properties for electromagnetic scattering in a two-layered medium, *Math. Method. Appl. Sci.*, **21** (1998), 433-461.

[17] M. Durán, I. Muga and J.-C. Nédélec, The Helmholtz equation with impedance in a half-plane, *CR Acad. Sci. Paris Ser. I*, **340** (2005), 483-488.

[18] G. Kristensson, Uniqueness theorem for Helmholtz equation: penetrable media with an infinite interface, *SIAM J. Math. Anal.*, **11** (1980), 1104-1116.

[19] Y. Xu, Radiation condition and scattering problem for the time-harmonic acoustic waves in a stratified medium with a nonstratified inhomogeneity, *IMA J. Appl. Math.*, **54** (1995), 9-29.

[20] B. Zhang and S.N. Chandler-Wilde, Acoustic scattering by an inhomogeneous layer on a rigid plate, *SIAM J. Appl. Math.*, **58** (1998), 1931-1950.

[21] J.P. Bérenger, A perfectly matched layer for the absorption of electromagnetic waves, *J. Comput. Phys.*, **114** (1994), 185-200.

[22] C. Rappaport and S. Winton, Using the PML ABC for air/soil wave interaction modeling in the time and frequency domains, *Int. J. Subsurface Sensing Technologies and Applications*, **1** (2000), 289–303.

[23] S.V. Tsynkov and E. Turkel, A Cartesian perfectly matched layer for the Helmholtz equation, in Absorbing Boundaries and Layers, Domain Decomposition Methods, Applications to Large Scale Computations, L. Tourrette and L. Halpern (Eds.), Nova Science Publishers, New York, 2001, 279-309.

[24] E. Turkel and A. Yefet, Absorbing PML boundary layers for wave-like equation, *App. Numer. Math.*, **27** (1998), 533-557.

[25] Y. Chen, Inverse scattering via Heisenberg uncertainty principle, *Inverse Problems*, **13** (1997) 253–282.

[26] G. Bao and P. Li, Inverse medium scattering problems for electromagnetic waves, *SIAM J. Appl. Math.*, **65** (2005), 2049-1066.

[27] G. Bao and J. Liu, Numerical solution of inverse problems with multi-experimental limited aperture data, *SIAM J. Sci. Comput.*, **25** (2003), 1102-1117.

[28] O. Dorn, H. Bertete-Aguirre, J.G. Berryman and G.C. Papanicolaou, A nonlinear inversion method for 3D electromagnetic imaging using adjoint fields, *Inverse Probl.*, **15** (1999), 1523-1558.

[29] O. Dorn, E. Miller and C. Rappaport, A shape reconstruction method for electromagnetic tomography using adjoint fields and level sets, *Inverse Probl.*, **16** (2000), 1119-1156.

[30] F. Natterer and F. Wübbeling, A propagation-backpropagation method for ultrasound tomography, *Inverse Probl.*, **11** (1995), 1225-1232.

[31] F. Natterer, An error bound for the Born approximation, *Inverse Probl.*, **20** (2004), 447-452.

[32] F. Natterer, Ultrasound tomography with fixed linear arrays of transducers, Institut für Numerische und Angewandte Mathematik, Universität Münster, preprint.

[33] H. Engl, M. Hanke and A. Neubauer, Regularization of Inverse Problems, Kluwer, Dordrecht, 1996.

[34] J. Coyle, Locating the support of objects contained in a two-layered background medium in two dimensions, *Inverse Probl.*, **16** (2000), 275-292.

[35] C.M. Linton, The Green's function for the two-dimensional Helmholtz equation in periodic domains, *J. Engrg. Math.*, **33** (1998), 377-402.

[36] C.M. Linton and D.V. Evans, The radiation and scattering of surface waves by a vertical circular cylinder in a channel, *Philos. Trans. R. Soc. A*, **338** (1992), 325-357.